Published in "Structure 20(12): 2151–2160, 2012"
which should be cited to refer to this work.

Ego3 Functions as a Homodimer to Mediate the Interaction between Gtr1-Gtr2 and Ego1 in the EGO Complex to Activate TORC1

Tianlong Zhang,[1,3] Marie-Pierre Péli-Gulli,[2,3] Hui Yang,[1] Claudio De Virgilio,[2,*] and Jianping Ding[1,*]
[1]State Key Laboratory of Molecular Biology, Institute of Biochemistry and Cell Biology, Shanghai Institutes for Biological Sciences, Chinese Academy of Sciences, 320 Yue-Yang Road, Shanghai 200031, China
[2]Division of Biochemistry, Department of Biology, University of Fribourg, CH-1700 Fribourg, Switzerland
[3]These authors contributed equally to this work
*Correspondence: claudio.devirgilio@unifr.ch (C.D.V.), jpding@sibs.ac.cn (J.D.)

SUMMARY

The yeast EGO complex, consisting of Gtr1, Gtr2, Ego1, and Ego3, localizes to the endosomal and vacuolar membranes and plays a pivotal role in cell growth and autophagy regulation through relaying amino acid signals to activate TORC1. Here, we report the crystal structures of a wild-type and a mutant form of *Saccharomyces cerevisiae* Ego3. Ego3 assumes a homodimeric structure similar to that of the mammalian MP1-p14 heterodimer and the C-terminal domains of the yeast Gtr1-Gtr2 heterodimer, both of which function in TORC1 signaling. Structural and genetic data demonstrate that the unique dimer conformation of Ego3 is essential for the integrity and function of the EGO complex. Structural and functional data also identify a potential binding site for Gtr1-Gtr2. These results suggest a structural conservation of the protein components involved in amino acid signaling to TORC1 and reveal structural insights into the molecular mechanism of Ego3 function in TORC1 signaling.

INTRODUCTION

The target of rapamycin (TOR) proteins are structurally and functionally conserved from yeast to human and belong to the phosphoinositide 3-kinase-related kinase family (Keith and Schreiber, 1995). The mammalian TOR (mTOR) and its orthologs are central regulators of cell growth, proliferation, and differentiation, and have been implicated in many diseases including cancers and diabetes. In all eukaryotes, TOR exists in two distinct multiprotein complexes, TOR complex 1 (TORC1) and TOR complex 2 (TORC2) (Kim et al., 2002; Loewith et al., 2002). In yeast, TORC1 contains Tor1 or Tor2, Kog1, Lst8, and Tco89 (Loewith et al., 2002; Reinke et al., 2004). TORC1 is sensitive to growth factors, energy status, and amino acid supply and functions as a regulator of transcription, protein translation, ribosomal biogenesis, and autophagy (De Virgilio and Loewith, 2006; Guertin and Sabatini, 2007).

Amino acids are potent activators of TORC1 and stimulate the phosphorylation of TORC1 substrates such as S6Ks and 4EBPs in mammals and Sch9 in yeast (Hara et al., 1998; Urban et al., 2007). The conserved Rag GTPases integrate lysosomal amino acid signals via the vacuolar ATPase (Zoncu et al., 2011), and/or cytoplasmic leucine levels via the leucyl-tRNA synthetase (Bonfils et al., 2012; Han et al., 2012), to control TORC1 function (Binda et al., 2009; Dubouloz et al., 2005; Kim et al., 2008; Sancak et al., 2008).

Mammalian cells contain four Rag GTPases, which form heterodimers of either RagA or RagB with either RagC or RagD (Schürmann et al., 1995; Sekiguchi et al., 2001). Rag GTPases do not directly stimulate the kinase activity of mTORC1 in vitro, but regulate the intracellular localization of mTORC1 (Sancak et al., 2008). Amino acid signals induce RagA/B to bind GTP, and the corresponding heterodimers interact with Raptor and mediate relocation of mTORC1 to Rab7-positive vesicles (late endosomes and lysosomes) where mTORC1 can be activated by the small GTPase Rheb (Sancak et al., 2008). No obvious lipid modification signals for membrane attachment have been found in the amino acid sequences of Rag GTPases. Recently, however, it was shown that the Ragulator complex consisting of p18/LAMTOR1, p14/LAMTOR2, MP1/LAMTOR3, C7orf59/LAMTOR4, and HBXIP/LAMTOR5, interacts with the Rag GTPases and mediates mTORC1 translocation to lysosomal membranes in response to amino acids (Sancak et al., 2010; Bar-Peled et al., 2012). MP1 and p14 form an almost symmetrical heterodimer and are anchored to late endosomes or lysosomes by p18 through its N-terminal lipid modification (Kurzbauer et al., 2004; Lunin et al., 2004; Nada et al., 2009; Sancak et al., 2010).

Saccharomyces cerevisiae cells express a single Rag GTPase heterodimer, namely, Gtr1-Gtr2, which forms, together with Ego1/Meh1 and Ego3/Slm4, the EGO complex (EGOC) that localizes to the vacuolar membrane (Dubouloz et al., 2005). Depletion of any of the EGOC components leads to failure in recovery from rapamycin-induced growth arrest and causes low TORC1 activity, indicating that these proteins play an important role in cell growth regulation upstream of TORC1 (Binda et al., 2009; Dubouloz et al., 2005). In line with this assumption, GTP-bound Gtr1 combines with GDP-bound Gtr2 to interact with and activate TORC1 via a still elusive mechanism (Binda et al., 2009). Analogous to the role of p18 in the Ragulator

Table 1. Summary of Diffraction Data and Structure Refinement Statistics

	I-Derivative	Wild-type	M1 Mutant
Diffraction Data			
Wavelength (Å)	1.7712	0.9791	0.9794
Space group	$C222_1$	$C222_1$	$P4_3$
Cell parameters			
a (Å)	61.52	61.96	60.53
b (Å)	99.13	99.31	60.53
c (Å)	158.58	156.11	116.85
Resolution (Å)	50.0–2.70	50.0–2.10	50.0–2.60
	(2.80–2.70)[a]	(2.18–2.10)	(2.69–2.60)
Observed reflections	89,071	135,634	58,777
Unique reflections ($I/\sigma(I) > 0$)	13,889	28,959	12,915
Average redundancy	6.4 (4.4)	4.7 (4.1)	4.6 (4.5)
Average $I/\sigma(I)$	21.9 (3.1)	17.1 (2.2)	15.5 (3.4)
Completeness (%)	98.8 (92.3)	99.5 (98.8)	99.7 (99.6)
R_{merge} (%)	10.9 (44.6)	8.8 (44.4)	14.7 (43.1)
Refinement and Structure Model			
Reflections ($Fo \geq 0\sigma(Fo)$)			
Working set		27,380	12,218
Test set		1,448	649
R_{work}/R_{Free} (%/%)		17.3/22.1	20.8/25.2
No. of protein atoms		2,475	2,234
No. of water atoms		147	52
Average B factor (Å^2)			
All atoms		53.0	47.1
Main chain		49.0	44.7
Side chain		56.7	47.4
Water		54.9	49.8
Rmsd			
Bond lengths (Å)		0.008	0.008
Bond angles (°)		1.1	1.2
Ramachandran plot (%)[b]			
Favored		96.7	97.4
Allowed		100.0	100.0

[a]Numbers in parentheses represent the highest resolution shell.
[b]Statistics of the Ramachandran plot was analyzed using MolProbity.

complex in higher eukaryotes, the N-myristoylated Ego1 may serve to properly tether Gtr1-Gtr2 to the vacuolar/lysosomal membrane for proper TORC1 activation (Ashrafi et al., 1998; Kogan et al., 2010), while the role of Ego3 in this process is still poorly understood.

In this study, we report the crystal structure of *S. cerevisiae* Ego3, which significantly differs from the previously published Ego3 crystal structure that forms a dimer of dimers, or a tetramer (Kogan et al., 2010). Notably, we show that Ego3 assumes a homodimeric structure, which is very similar to both the mammalian MP1-p14 heterodimer in the Ragulator complex and the C-terminal domains of the yeast Gtr1-Gtr2 heterodimer. In addition, structural and functional analyses of Ego3 and Ego3 variants demonstrate that the unique dimer conformation of Ego3 is essential for proper control of TORC1 activity.

RESULTS AND DISCUSSION

Overall Structure of the Ego3 Homodimer

The crystal structure of Ego3 was solved using the single isomorphous replacement with anomalous scattering (SIRAS) method with the anomalous scattering of I and refined to 2.1 Å resolution in space group $C222_1$, yielding a R_{work} of 17.3% and a R_{free} of 22.1% (Table 1). There are two Ego3 molecules in an asymmetric unit forming a homodimer with a 2-fold noncrystallographic symmetry (NCS) (Figure 1A), which is consistent with the results of size-exclusion chromatography showing that Ego3 exists as a homodimer in solution (Figure S1available online). The two Ego3 monomers (hereafter designated as A and B) adopt an almost identical overall structure with an rmsd of 0.6 Å for 152 Cα atoms. The full-length Ego3 consists of 162 residues with a theoretical molecular mass of 18 kDa. The final structure model of the dimeric Ego3 contains the whole polypeptides except the N-terminal residues 1–4 and the C-terminal 6xHis tag in monomer A, and the N-terminal residues 1–4, residues 53–56 of a surface exposed loop, and the C-terminal 6xHis tag in monomer B. Thus, monomer A with more detectable residues is chosen for structural analysis and discussion unless otherwise specified.

The Ego3 monomer consists of a central core β sheet of six antiparallel β strands (β2-β1-β6-β5-β4-β3) flanked by helix α2 on one side and helices α3 and α1′ of the other monomer (hereafter components of the other monomer are designated by apostrophes) on the other side (Figure 1A). The Ego3 dimer has two unique structural features: the core β sheets of the two monomers are related by the 2-fold NCS to form an extended 12 stranded antiparallel β sheet; the N-terminal helix α1 of one monomer reaches over the other monomer via a long α1/β1 loop to form a swapping conformation (Figure 1A).

A Unique Dimer Interface

The two Ego3 monomers in the asymmetric unit form a homodimer. The dimer interface is formed mainly by helices α1 and α3, the α1/β1 loop, and strands β1, β2, β3, and β6 of both monomers, which involves 20 hydrogen bonds and numerous hydrophobic interactions (Table S1) and buries 2,092 Å^2 or 20.3% of the total solvent accessible surface area as analyzed by the PROTORP server (Reynolds et al., 2009). The interface is composed of three regions (Figure 1B). In region I, the swapping helix α1′ of monomer B stretches into a hydrophobic groove formed by helix α3 and strands β1, β2, and β6 of monomer A and makes three hydrogen-bonding interactions and numerous hydrophobic contacts with residues of monomer A (Figure 1B, left panel; Table S1). With the 2-fold NCS of the homodimer, the swapping helix α1 of monomer A has similar interactions with the same structure elements of monomer B. In region II, the N-terminal of helix α3 and the α1/β1 loop of one monomer interact with the corresponding structure elements of the other via eight hydrogen bonds and a number of hydrophobic contacts, and vice versa (Figure 1B, middle panel; Table S1). The α1/β1 loops of the two monomers contribute nearly one-half of the hydrophilic interactions and one-third of the hydrophobic contacts at the dimer interface. Region III is formed between the N termini of the two β3 strands of the two monomers via five hydrogen bonds and several hydrophobic contacts

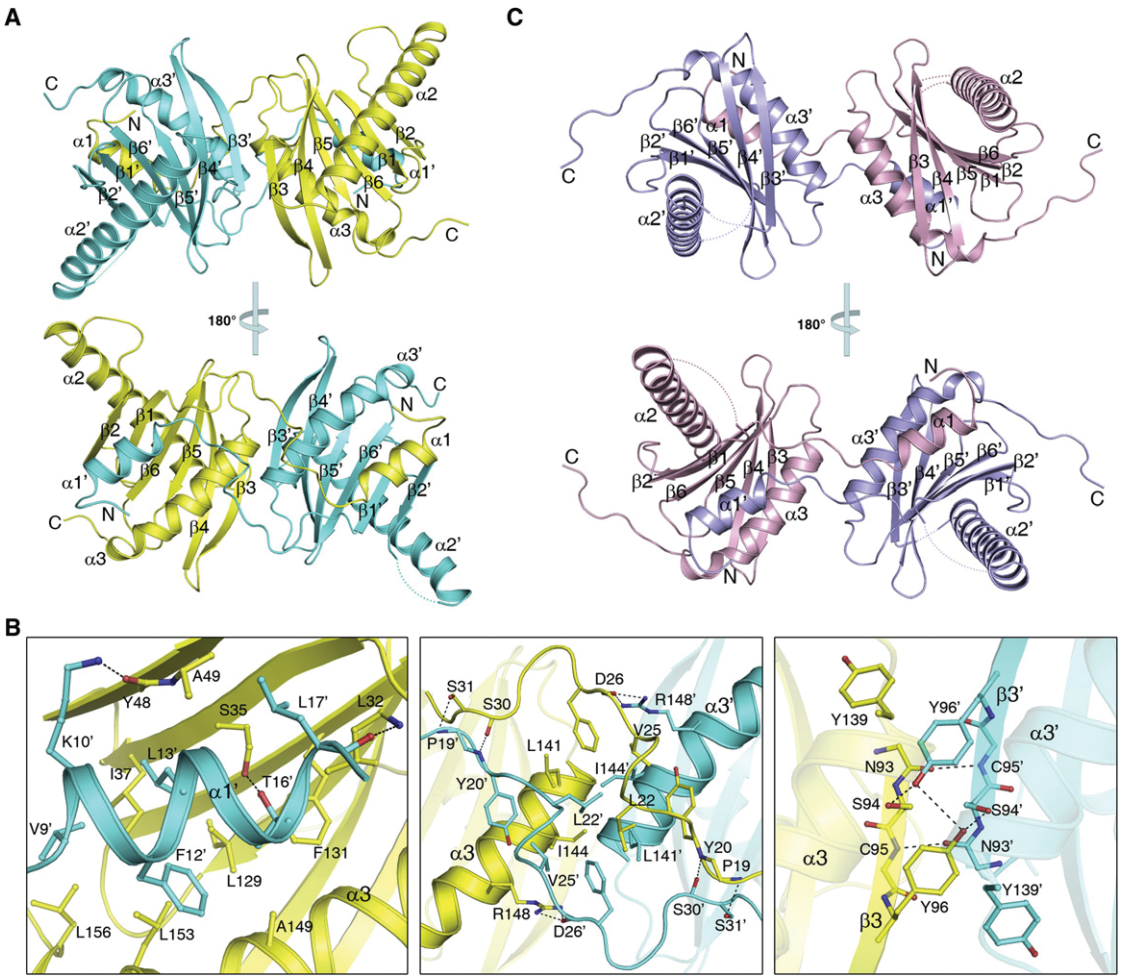

Figure 1. Crystal Structure of the Ego3 Homodimer

(A) Ribbon representation of the Ego3 homodimer with monomer A in yellow and monomer B in cyan.

(B) Interactions at the Ego3 homodimer interface. Hydrogen bonds are indicated with dashed lines. Left panel: Interactions of the swapping helix α1′ with residues of monomer A. Middle panel: Interactions between helix α3 and the α1/β1 loop of the two monomers. Right panel: Interactions between the N-terminal part of strand β3 of the two monomers.

(C) Ribbon representation of the Ego3-M1 homodimer with one monomer in pink and the other in light blue.

See also Table S1 and Figures S1, S2, and S5.

(Figure 1B, right panel; Table S1). In particular, Tyr96 contributes more than half of the hydrophilic and hydrophobic contacts in this region.

Sequence alignment of Ego3 from different species shows that most of the residues of helices α1 and α3, and strands β1, β2, β3, and β6 that are involved in the hydrophilic and hydrophobic contacts at the dimer interface are strictly or highly conserved, including Val9, Phe12, Leu13, and Leu17 of helix α1, Ser35 and Ile37 of strand β1, Ser47 and Tyr48 of strand β2, Ser94, Cys95, and Tyr96 of strand β3, Leu129 of strand β6, and Tyr139, Gly140, Leu141, and Lys145 of helix α3 (Figure S2A). Although the residues of the α1/β1 loop are not conserved, the lengths of the α1/β1 loop (12–15 residues) are comparable (Figure S2A). These conservations suggest that the homodimeric architecture with a swapping conformation of Ego3 might exist in other species and is essential for its biological function. In particular, the α1/β1 loop appears to play a critical role in the formation of the swapping conformation of the dimer and thus might play an important role in Ego3 function.

Comparison of the Ego3 Dimer with Other Roadblock/LC7 Domain-Containing Proteins

A structural similarity search in the Protein Data Bank using the Dali server (Holm and Rosenström, 2010) reveals that Ego3 has a high structural similarity to members of the Roadblock/LC7 superfamily (Koonin and Aravind, 2000). This family includes the C-terminal domains of Gtr1 and Gtr2, MP1, p14, and the recently discovered C7orf59/LAMTOR4 and HBXIP/LAMTOR5, which all participate in TORC1 signaling (Cui et al., 2008; Gong et al., 2011; Kurzbauer et al., 2004; Lunin et al., 2004; Sancak et al., 2010; Bar-Peled et al., 2012) as well as a GTPase-activating protein (GAP) MglB homodimer (Miertzschke et al., 2011). For instance, superposition of Ego3 with MP1 and p14 in the MP1-p14 complex (PDB code 1VET) yields an rmsd of

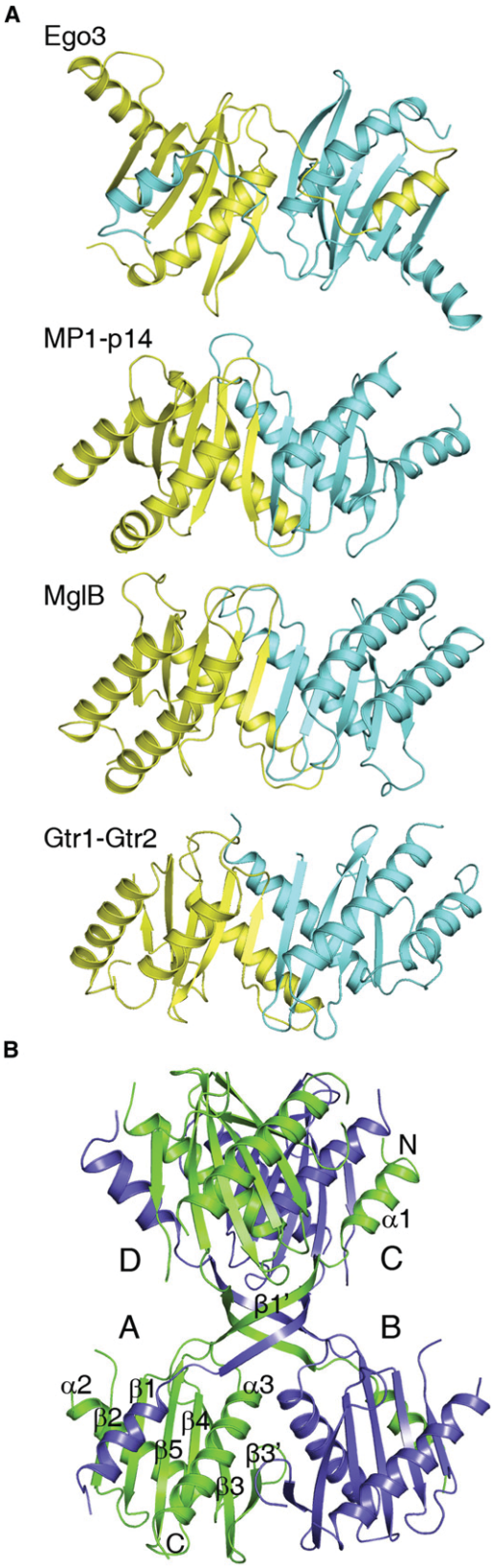

Figure 2. Structural Comparison of the Ego3 Dimer, the Other Roadblock/LC7 Domain-Containing Proteins, and the Ego3 Tetramer

(A) Ribbon representation of the Ego3 dimer and three Roadblock/LC7 domain-containing proteins, namely, the MP1-p14 heterodimer (PDB code 1VET), the MglB homodimer (PDB code 3T1S), and the C-terminal domains of the Gtr1-Gtr2 heterodimer (PDB code 3R7W).

(B) Ribbon representation of the Ego3 tetramer (PDB code 3LGO). In a dimer, one monomer is colored in green and the other in blue. Two adjacent dimers associate with each other to form a tetramer. The nomenclature of the secondary structures is after that by Kogan et al. (2010).

See also Figures S2 and S3.

2.2 Å (80 Cα atoms) and 1.5 Å (84 Cα atoms), respectively. Interestingly, detailed structural comparisons show that the Ego3 homodimer has a similar architecture to the MP1-p14 heterodimer (Kurzbauer et al., 2004; Lunin et al., 2004), the dimeric C-terminal domains of the Gtr1-Gtr2 heterodimer (Gong et al., 2011), and the MglB homodimer (Miertzschke et al., 2011) (Figure 2A). Despite a low sequence similarity, MP1 and p14 adopt a nearly identical overall structure and form an almost symmetrical heterodimer (Kurzbauer et al., 2004; Lunin et al., 2004); the same holds true for the C-terminal domains of Gtr1 and Gtr2 (Gong et al., 2011). Nevertheless, there are some notable differences between the Ego3 homodimer and the MP1-p14 and Gtr1-Gtr2 heterodimers and the MglB homodimer. Specifically, Ego3 has a swapping helix α1, a long α1/β1 loop (15 residues in Ego3, 4 residues in MP1, 5 residues in p14, 2 residues in Gtr1, 3 residues in Gtr2, and 2 residues in MglB), an extra β strand (β3), and a bent central β sheet (Figure S2B). These structural differences make the Ego3 dimer adopt a twisted dimer conformation such that the β3 strands of the two monomers have fewer interactions with each other at the dimer interface, and the α2 helices of the two monomers are positioned far apart without any interaction (Figure 2A). However, the dimer interface of Ego3 is augmented by the swapping of helix α1 and the following α1/β1 loop and the interactions of the α3 helices of the two monomers. Considering that the MP1-p14 heterodimer, the Gtr1-Gtr2 heterodimer, and the MglB homodimer function as dimers, the similarity of the dimeric architecture of Ego3 to these proteins suggests that dimerization of Ego3 is essential for its biological function.

Comparison of the Ego3 Dimer with the Ego3 Tetramer

Recently, a crystal structure of Ego3 was reported in which Ego3 forms a tetramer (PDB code 3LGO) (Kogan et al., 2010) (Figure 2B). Structural comparison shows that although the overall structures of the Ego3 monomers in the homodimer and homotetramer are very similar with an rmsd of 1.3 Å for about 112 Cα atoms (superposition without the N-terminal helix α1 and the following α1/β1 loop), the assemblies of the dimer and the tetramer are significantly different, particularly in the swapping of helix α1 and the conformation of the α1/β1 loop region (Figures 2B and S3). In the structure of the Ego3 tetramer, an asymmetric unit contains one monomer and four crystallographic symmetry-related monomers form a dimer of dimers or a tetramer. The dimeric interface between monomers A and B (or C and D) involves largely hydrophobic interactions between strand β3 and helix α3 of each monomer and buries a total of 775 Å solvent-accessible surface areas (Figure S3A). This dimeric interface is quite different from that in our Ego3 dimer: although

strand β3 and helix α3 are involved in formation of the dimeric interface in both cases, the orientations of these structure elements, the interaction modes, and the residues contributing to the interactions are completely different (Figure S3A). If one monomer is superimposed, the other would have a rotation of 116° relative to each other (Figure S3B). In the Ego3 dimer, the N-terminal parts of strand β3 of the two monomers interact with each other via several hydrogen bonds, leading to the formation of an extended, intermolecular β sheet. In the Ego3 tetramer, however, no hydrogen-bonding interactions exist between the β3 strands of the two monomers and thus no continuous, intermolecular β sheet is formed. There is only one hydrogen bond between the side chain of Tyr96 in strand β3 of monomer A and the side chain of Arg148 in helix α3 of monomer B at this interface. As Arg148 is not conserved in different species (Figure S2A), the significance of this hydrogen-bonding interaction is not clear. Moreover, the distance between the negatively charged side-chain carboxyls of Glu99 of the two monomers is very close (2.3 Å) which may only be permitted by the special crystallization condition of the Ego3 tetramer (Kogan et al., 2010). In the Ego3 tetramer, the tetrameric interface between the two dimers A/B and C/D is mediated mainly through the α1/β1 loop region and the swapping helix α1. The N-terminal helix α1 is swapped between monomers A and C (and between monomers B and D); the α1/β1 loop region forms a β strand which associates with the equivalents of the other three monomers to form a four stranded, orthogonal β sheet (Figure 2B). This is also quite different from the Ego3 dimer in which the N-terminal helix α1 is swapped between two adjacent monomers A and B, and the long α1/β1 loop lies on the surface and connects helix α1 back to its monomer. Thus, the question arises whether the Ego3 dimer or tetramer is the functional unit or is biologically relevant.

Biological Relevance of the Ego3 Dimer

To investigate the biological relevance of the Ego3 dimer and/or tetramer, we first examined the oligomeric state of Ego3 in solution using size-exclusion chromatography. Previously, Kogan et al. reported that the equilibrium analytical ultracentrifugation data suggested that Ego3 assumes a mixture of different oligomeric states; however, the size-exclusion chromatography data showed that Ego3 attached with or without an N-terminal 6xHis tag exists in a single oligomeric state with a molecular mass in the range of 25–43 kDa (Kogan et al., 2010). Consistently, our size-exclusion chromatography data also showed that the wild-type Ego3 exhibited a single peak with a molecular mass in the range of 25–43 kDa (Figure S1). These results indicate that Ego3 exists as a dimer rather than a tetramer or a mixture of different oligomeric states in solution, which is in agreement with our structural data. The discrepancy between the equilibrium analytical ultracentrifugation and the size-exclusion chromatography results by Kogan et al. is unclear. The Ego3 protein has an N-terminal 6xHis tag in Kogan et al., but a C-terminal 6xHis tag in this study. In the structure of the Ego3 tetramer, both the N and C termini of Ego3 are not involved in dimer or tetramer formation. In the structure of the Ego3 dimer, the swapping N terminus is involved in interactions with the other monomer but the C terminus is not involved in dimer formation. Thus, the positions of the 6xHis tag should have no effects on the formation of the dimer or the tetramer.

The crystals of the Ego3 tetramer were grown in a crystallization solution containing 200–350 mM L-arginine and at a very low pH 3.0 (Kogan et al., 2010). L-arginine is often used as a versatile solvent additive, which is helpful for protein refolding and aggregation suppression. L-arginine at high concentration (i.e., 1 M) can interact with the side chains of almost all amino acids and can reduce hydrogen-bonding and ionic interactions as well as hydrophobic interactions at protein-protein interfaces (Arakawa et al., 2007). In addition, the pH value can also have a great effect on protein-protein interactions. At acidic pH conditions, some ionizable groups, such as the side-chain hydroxyl of Tyr, would be protonated and more hydrophobic. Thus, an acidic pH may induce conformational changes of the tertiary structure by reduction of hydrophilic interactions and/or introduction of hydrophobic interactions. For example, an amidase from the hyperthermophilic archaeon *Sulfolobus solfataricus* forms a dimer at pH above 8.0 but an octamer at pH below 3.0 (D'Abusco et al., 2005). Thus, it appears to be very likely that the formation of the Ego3 tetramer is an artifact caused by the special crystallization condition, particularly the high concentration of L-arginine and very acidic pH. In other words, the Ego3 tetramer is unlikely to be biologically relevant.

Additionally, as discussed above, structural comparison shows that the Ego3 dimer has a similar architecture to the MP1-p14 heterodimer and the C-terminal domains of the Gtr1-Gtr2 heterodimer, both of which function as dimers in the TORC1 signaling pathway. Furthermore, sequence comparison shows that most of the residues involved in the formation of the Ego3 dimer interface are strictly or highly conserved. Taken all of these results together, we conclude that the Ego3 dimer is the functional, biologically relevant unit.

Functional Importance of the Ego3 Dimer

To investigate whether the unique dimer conformation of Ego3 is required for its function, five mutants named Ego3-M0, Ego3-M1, Ego3-M2, Ego3-M3, and Ego3-M8 were generated (for details, see Table S2). Among these, Ego3-M1, Ego3-M3 and Ego3-M8 were selected for further analyses based on their mislocalization and increased sensitivity to rapamycin treatment in the initial characterization (Figures S4A and S4B). Basically, in the Ego3-M1 mutant, the long α1/β1 loop is shortened such that residues KPYDLHSVDFKTSSL are substituted with KPYGSL. A conserved Tyr (Tyr96), located in strand β3, was found to be involved in several hydrophilic and hydrophobic interactions in region III of the dimeric interface. The Ego3-M3 variant contains the same shortened α1/β1 loop as Ego3-M1 and additionally a mutation of this specific Tyr to Glu (Y96E). Of note, the Y96E mutation on its own (Ego3-M2) had no significant impact on Ego3-GFP localization or rapamycin-sensitivity of the corresponding cells (Figure S4). Finally, in the Ego3-M8 mutant, the N-terminal 17 residues including the swapping helix α1 are deleted which was expected to prevent stable homodimer formation.

Attempts to produce recombinant Ego3-M3 and Ego3-M8 proteins have remained unsuccessful (both were expressed as inclusion bodies), thereby precluding further in vitro structural analysis on these mutants. On the other hand, recombinant Ego3-M1 was expressed normally and displayed an unchanged

oligomeric state in solution as judged from size-exclusion chromatography analysis (Figure S1). We therefore went on to determine the crystal structure of Ego3-M1.

The crystal structure of Ego3-M1 was solved using the molecular replacement (MR) method and refined to 2.6 Å resolution in space group $P4_3$, yielding a R_{work} of 20.8% and a R_{free} of 25.2% (Table 1). There are also two Ego3-M1 molecules in an asymmetric unit forming a homodimer with a 2-fold NCS (Figure 1C). Superposition of the two Ego3-M1 monomers yields an rmsd of 0.2 Å for 139 Cα atoms. The final structure model of the Ego3-M1 dimer contains residues 6–156 of monomer A except for residues 44–48 and 78–83, and residues 6–156 of monomer B except for residues 44–48 and 80–82.

The Ego3-M1 monomer has an overall structure very similar to that of the wild-type Ego3 monomer; however, the dimer conformation of Ego3-M1 is significantly different from that of the wild-type Ego3 (Figures 1A and 1C). If we superpose one monomer of the Ego3 and Ego3-M1 dimers, the other monomer in the Ego3-M1 dimer has a rotation of 86° in relation to that in the Ego3 dimer (Figure S5). Due to the shortening of the α1/β1 loop, the two monomers rotate toward each other along the axis vertical to the 2-fold NCS. Although the N-terminal α1 helix in Ego3-M1 maintains a swapping configuration and has interactions with several structure elements of the other monomer similar to that in the wild-type Ego3, the two α1 helices and the side of the dimer where the α1/β1 loops are located, are pulled much closer to each other. Concurrently, the central β sheets and the α2 helices of the monomers rotate away from each other and are no longer interacting. As a result, the two monomers are linked together mainly by the swapping α1 helix and the α1/β1 loop of both monomers and the dimer interface is much looser compared to that in the wild-type Ego3. In other words, although Ego3-M1 forms a dimer, the dimer interface is significantly distorted, altering its surface properties.

Next, we analyzed the capacities of the Ego3 variants to homodimerize and bind to the other EGOC components in vivo using the membrane-based split-ubiquitin two-hybrid system. In line with our in vitro data, we found that Ego3-M1 could homodimerize (Figure 3A). However, the presence of the additional Y96E mutation in Ego3-M3 largely impaired its dimerization. Absence of the swapping helix α1 also prevented dimerization of Ego3-M8 (Figure 3A). Furthermore, regardless of whether they could dimerize or not, these mutants failed to interact with the vacuolar anchor Ego1 (Figure 3A), and consequently failed to accumulate at the vacuolar periphery (Figure 3B). In addition, all of these Ego3 mutants failed to associate with the GTP-locked forms of Gtr1 and Gtr2 (Figures 3A), which turned out to be the best Ego3-interacting forms in the two-hybrid system (data not shown). Moreover, Ego3-M3-GFP did not coprecipitate with Gtr1-WT-TAP in pull-down experiment (Figure 3C). In parallel, we examined the subcellular localization of Gtr1-WT-GFP in cells expressing these *ego3* mutants (Figure 3D). In cells expressing the *ego3-M1* mutant, Gtr1-WT-GFP could still concentrate at the vacuolar membrane albeit to a lesser extent. In cells expressing the impaired dimerization mutants (*ego3-M3* and *ego3-M8*), like in *ego3Δ* cells, Gtr1-WT-GFP displayed a diffuse cytoplasmic staining (Figure 3D). Altogether, these results suggest that dimerization of Ego3 is necessary but not sufficient for association with its partners and localization to the vacuolar membrane; instead, its unique dimer conformation and surface properties matter.

Both abrogation of dimerization or alteration of the dimer surface of Ego3 affect its capacity to interact with the other EGOC components, and hence may affect proper EGOC-mediated TORC1 signaling. To test this possibility, we compared the abilities of the untagged Ego3 mutants to suppress the growth defect and TORC1 activity defect of the *ego3Δ* strain (Figures 4A and 4B). While Ego3-M1 exhibited partial rapamycin sensitivity compared to the other Ego3 variants tested, all of them failed to recover from a 6 hr rapamycin treatment (Figure 4A). Furthermore, leucine-starved cells responded less promptly (Ego3-M1) or failed to respond to leucine restimulation (other mutants) (Figure 4B), therefore confirming the importance of the unique dimer conformation of Ego3 for optimal EGOC-mediated TORC1 activation.

A Potential Binding Site for Other Components of the EGO Complex

Previous biological data have shown that Ego3 interacts with Ego1 and Gtr1-Gtr2 to form the EGO complex (Dubouloz et al., 2005; Gao and Kaiser, 2006). Our structural data in combination with the mutagenesis data have further shown that the unique dimer conformation of Ego3 is essential for its function and its interactions with Ego1 and Gtr1-Gtr2. Thus, we were tempted to identify potential binding site(s) for these protein partners on Ego3. Sequence comparison shows that Ego3 is conserved in different species (Figure S2A); the residues on the surface side where helix α2 is located are more conserved than these on the surface side where helix α1 and the α1/β1 loop are located, and particularly, there are a number of strictly or highly conserved residues in helix α2 and the β4/β5 loop on the same side (Figure S6). We speculated that these conserved regions might be potential binding site(s) for Ego1 and/or Gtr1-Gtr2, and thus constructed several Ego3 mutants containing multiple mutations in these regions including Ego3-M4, Ego3-M5, Ego3-M6, and Ego3-M7 (for details, see Table S2 and Figure S6). Ego3-M4 was the only one to show some rapamycin sensitivity (Figure S4) and was therefore selected for further analyses (Figures 3 and 4). Ego3-M4 harbors a quadruple mutation (N67A/N68A/K70A/M71A) in the N-terminal part of helix α2. Recombinant Ego3-M4 exhibited an unchanged oligomeric state in solution (Figure S1). Consistent with this, Ego3-M4 was able to homodimerize in two-hybrid assay (Figure 3A). It also interacted with Ego1 (Figure 3A), and as expected, localized to the vacuolar membrane (Figure 3B). However, it showed reduced binding to Gtr2 (Figure 3A) and Gtr1 (Figures 3A and 3C). In agreement with this finding, Gtr1-WT-GFP was not recruited to the vacuolar membrane in cells expressing Ego3-M4 (Figure 3D). Altogether, these results suggest that the N-terminal region of helix α2 participates in the binding to Gtr1-Gtr2 and the four mutations in Ego3-M4 impair its binding to the Gtr GTPases.

Possible Functional Roles of Ego3 in TORC1 Activation

The EGO complex functions upstream of TORC1 signaling (Binda et al., 2009). Loss of any of the EGOC components or the TORC1 subunit Tco89 results in an inability to recover from

A

	Ego3-WT	Ego3-M1	Ego3-M3	Ego3-M8	Ego3-M4	Control	Ego1	Gtr1-GTP	Gtr2-GTP
Ego3-WT	17.3±1.5	n.d.	n.d.	n.d.	n.d.	0.9±0.1	69.5±2.5	236.6±14.7	10.9±0.6
Ego3-M1	n.d.	26.4±0.3	n.d.	n.d.	n.d.	0.3±0.1	4.5±1.0	10.2±2.2	1.1±0.1
Ego3-M3	n.d.	n.d.	5.9±0.5	n.d.	n.d.	0.2±0.1	2.8±0.3	1.7±0.2	0.3±0.1
Ego3-M8	n.d.	n.d.	n.d.	3.1±0.3	n.d.	0.2±0.1	2.9±0.3	4.0±0.5	0.5±0.1
Ego3-M4	n.d.	n.d.	n.d.	n.d.	12.9±1.1	0.8±0.2	70.3±3.2	40.5±3.5	3.7±0.2
Control	2.7±0.4	2.7±0.3	1.3±0.2	0.6±0.1	0.6±0.1	n.d.	2.2±0.3	1.0±0.1	0.3±0.1

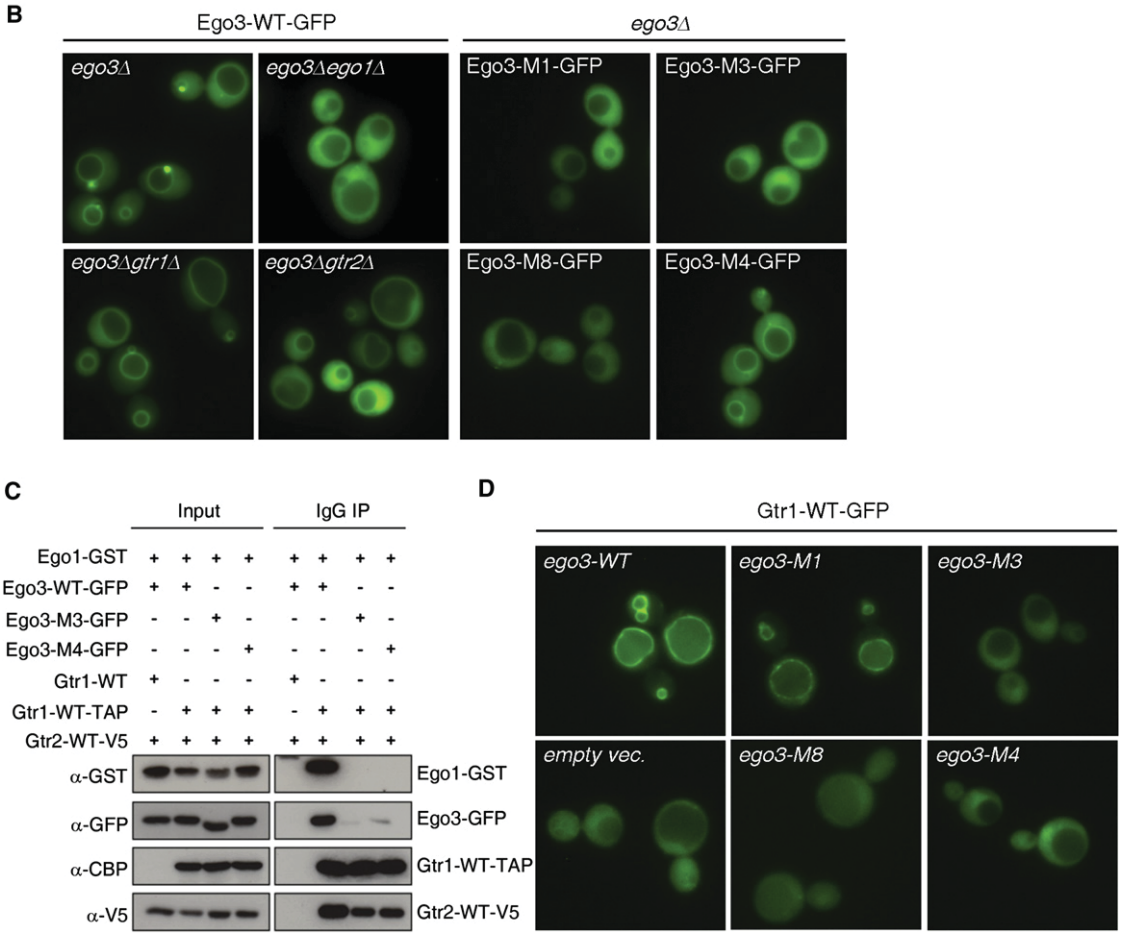

Figure 3. Ego3 Relies on Its Unique Dimer Conformation and Surface Properties to Interact with Its EGOC Partners and Localize to the Vacuolar Membrane

(A) Interactions of the Ego3 variants (baits) with the same Ego3 variants, or with Ego1, Gtr1-GTP, or Gtr2-GTP (preys) were assessed using the split ubiquitin-based membrane two-hybrid system (Dualsystems Biotech). For each combination tested, β-galactosidase activity is expressed in Miller units as mean ± SD from at least three independent transformants grown overnight at 30°C. Empty bait vector pCabWT and pDl2-Alg5 prey were used as negative controls. n.d., not determined.

(B) Localization of the wild-type and mutant Ego3-GFP. Left panel: Localization of Ego3-WT-GFP was examined in prototrophic *ego1Δ ego3Δ gtr1Δ gtr2Δ* cells complemented for all the other EGOC components except the one indicated. Right panel: Localization of the Ego3-GFP variants was assayed in prototrophic *ego3Δ* cells expressing the corresponding Ego3-GFP mutant protein.

(C) TAP pull-down assays were performed on lysates of cells expressing either untagged Gtr1-WT or Gtr1-WT-TAP together with the indicated mutant forms of Ego3-GFP, Gtr2-WT-V5, and Ego1-GST. Coprecipitated proteins were eluted by TEV cleavage. Input and pulldown fractions were analyzed by western blot and probed with the indicated antibodies.

(D) Localization of Gtr1-WT-GFP was examined in prototrophic *ego3Δ* cells expressing the indicated Ego3 variants.

See also Tables S2–S4 and Figures S1, S4, and S6.

rapamycin-induced growth arrest (Binda et al., 2009; Dubouloz et al., 2005). Recent studies have revealed the importance of several scaffold proteins in mTORC1 signaling in mammalian cells: p18/LAMTOR1, p14/LAMTOR2, MP1/LAMTOR3, C7orf59/LAMTOR4, and HBXIP/LAMTOR5 form an extended Ragulator complex which, with the Rag GTPases, serves as

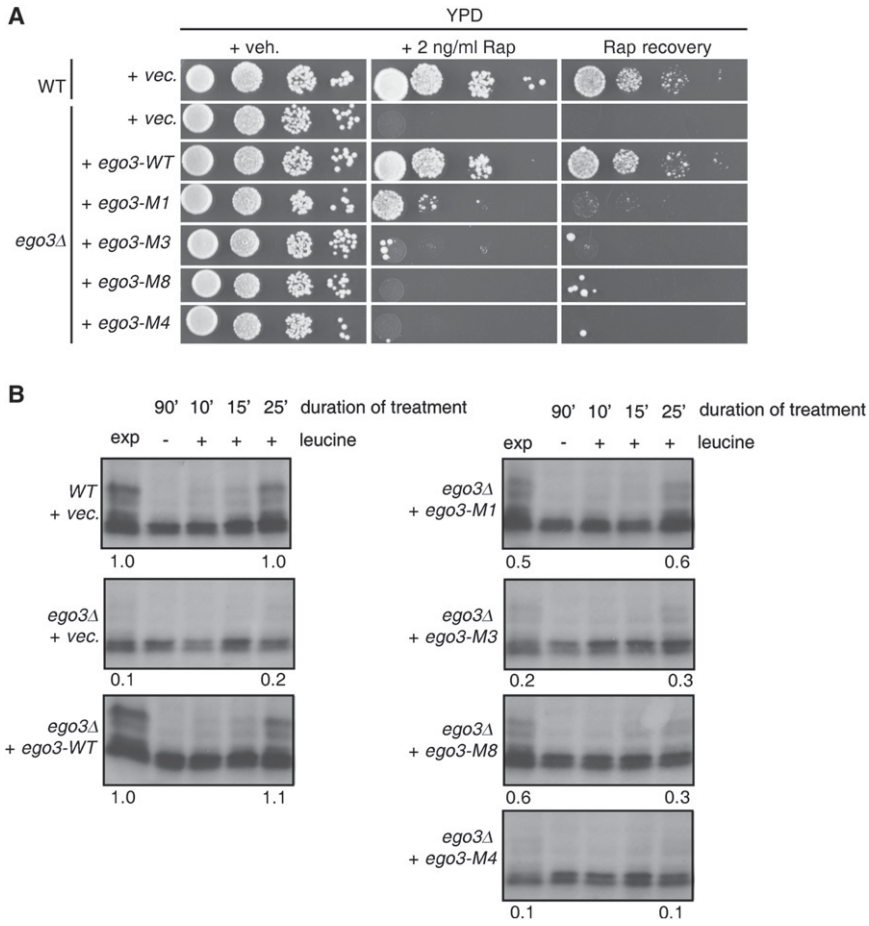

Figure 4. Ego3 Relies on Its Unique Dimer Conformation and Surface Properties to Mediate Adequate TORC1 Signaling

(A) Prototrophic WT and *ego3Δ* strains expressing the indicated Ego3 mutants were grown to exponential phase. Serial 10-fold dilutions were spotted on YPD supplemented with vehicle (veh.) or the indicated concentrations of rapamycin. Alternatively, they were treated for 6 hr with 200 ng/ml rapamycin, washed twice, and spotted on YPD (Rap recovery).

(B) In vivo TORC1 activity was assessed by monitoring the phosphorylation level of the TORC1 substrate Sch9 in the indicated leucine auxotrophic strains grown to exponential phase, starved for leucine for 90 min and restimulated with leucine (2.8 mM) for the indicated times. Numbers below represent TORC1 activity in either exponentially growing cells or cells restimulated with leucine for 25 min. *WT* TORC1 activity was set to 1 in each condition tested.

See also Tables S2–S4 and Figures S4 and S6.

a docking site for mTORC1 on lysosomal membrane (Sancak et al., 2010; Bar-Peled et al., 2012). MP1 and p14 prefer to form a heterodimer rather than homodimers (Lunin et al., 2004). The high structural conservation between the MP1-p14 heterodimer and the Ego3 homodimer suggests that the Ego3 homodimer might be the counterpart of the MP1-p14 heterodimer in yeast.

Based on our structural, biochemical and genetic data, we propose that the unique homodimer conformation of Ego3 is required for its binding to Ego1 and its recruitment to the vacuolar membrane. Moreover, the N-terminal region of its α2 helix represents a binding site for Gtr1-Gtr2, and is critical for the efficient docking of the Gtr GTPases to the vacuolar anchor Ego1. Interestingly, the extended form of the Ragulator complex has recently been found to exhibit GEF activity toward the Rag GTPases (Bar-Peled et al., 2012). We therefore suspect that, besides having a scaffolding role within EGOC, Ego3 may also work together with Ego1 and some other so-far-unidentified proteins to fulfill a regulatory function in TORC1 activation.

EXPERIMENTAL PROCEDURES

Cloning, Expression, and Purification of Proteins

The Ego3 open reading frame (ORF) was amplified by PCR from yeast genomic DNA and inserted into the NcoI and XhoI restriction sites of the pET-28a expression plasmid (Novagen) which attaches a 6xHis tag at the C terminus of the target protein. The plasmid was transformed into the *Escherichia coli* BL21 (DE3) strain. The transformed cells were grown at 37°C in lysogeny broth medium containing 0.05 mg/ml kanamycin until OD_{600} reached 0.8, and then induced with 0.5 mM isopropyl β-D-1-thiogalactopyranoside at 20°C for 20 hr. Cells were harvested and lysed by sonication in lysis buffer (30 mM Tris-HCl [pH 7.5] and 200 mM NaCl). 6xHis-tagged Ego3 was purified by affinity chromatography using a Ni-NTA column (QIAGEN) with the lysis buffer supplemented with 30 mM imidazole and 200 mM imidazole serving as washing buffer and elution buffer, respectively. The elution sample was further purified by gel filtration using a Superdex 75 10/300 (preparative grade) column (GE Healthcare) preequilibrated with storage buffer (10 mM HEPES [pH 7.5], 100 mM NaCl, 2 mM $MgCl_2$, and 1 mM DTT). The target protein was of sufficient purity (>95%) as determined by SDS-PAGE (12% gel).

Constructs of the *ego3* mutants containing point mutations, deletions, or substitutions were generated using the QuikChange Site-Directed Mutagenesis Kit (Strategene) or the TakaRa MutanBEST Mutagenesis Kit (TaKaRa Biotechnology) following the instruction manuals. Designs of the Ego3 mutants are summarized in Table S2. Expression and purification of the Ego3 mutants were performed as for the wild-type protein.

For construction of pRS414-*GTR2p-GTR2-WT-V5-6HIS,* the *GTR2* promoter and ORF without a stop codon were amplified by PCR from yeast genomic DNA and cloned in frame as a XhoI-BamHI fragment together with a BamHI-NotI PCR fragment encoding *V5-6HIS-CYC1* terminator into pRS414 digested with XhoI-NotI.

Crystallization, Data Collection, and Structure Determination

Crystallization of the wild-type Ego3 and the Ego3-M1 mutant was performed using the hanging drop vapor diffusion method by mixing 1.5 μl protein solution (about 15 mg/ml) and 1.5 μl reservoir solution at 4°C. Crystals of Ego3 were grown from drops consisting of a reservoir solution of 35% tacsimate (pH 7.0) after about 1 week. I-derivatized crystals were prepared by soaking the crystals of Ego3 in the crystallization solution containing 1 M NaI for 60 s. Crystals of Ego3-M1 were obtained from drops consisting of a reservoir solution of 1.6 M ammonium sulfate, 0.1 M MES monohydrate (pH 6.5), and 10% 1,4-dioxane. Single-wavelength anomalous dispersion diffraction data were collected to 2.7 Å resolution from a flash-cooled I-derivatized Ego3 crystal. Diffraction data for Ego3 and Ego3-M1 were collected

to 2.1 and 2.6 Å resolution, respectively, at −175°C at beamline 17U of Shanghai Synchrotron Radiation Facility (SSRF), China. The diffraction data were processed, integrated, and scaled together with HKL2000 (Otwinowski and Minor, 1997). The statistics of the diffraction data are summarized in Table 1.

The structure of Ego3 was solved using the SIRAS method implemented in Phenix (Adams et al., 2010). An initial model of 312 out of 324 residues of two Ego3 molecules and 131 water molecules was constructed automatically by ARP/wARP in warpNtrace mode (Perrakis et al., 1999). The remaining residues and additional water molecules were built manually using Coot (Emsley and Cowtan, 2004). The structure of Ego3-M1 was solved by the MR method implemented in Phenix. Structure refinement was carried out using Phenix and Refmac5 (Adams et al., 2010; Murshudov et al., 1997). The stereochemistry of the protein models was analyzed using MolProbity (Davis et al., 2007). Structure analysis was carried out using programs in CCP4 (Winn et al., 2011). The figures were generated using Pymol (http://www.pymol.org). The statistics of the structure refinement and the quality of the final structure models are summarized in Table 1.

Plasmids, Strains, and Growth Conditions

Plasmids used in this study are listed in Table S3. Cloning and site-directed mutagenesis were carried out following standard procedures. All constructs were verified by sequencing. Functionality of endogenously expressed untagged and tagged EGOC fusion proteins was confirmed by rapamycin sensitivity, recovery from rapamycin-induced growth arrest, and TORC1 activity assays.

S. cerevisiae strains used in this study are listed in Table S4. Prototrophic strains were used unless otherwise specified. Strains were grown to exponential phase at 30°C in synthetic defined medium with 2% glucose complemented with the appropriate nutrients for plasmid maintenance. When indicated (Rap recovery), they were treated with 200 ng/ml rapamycin for 6 hr at 30°C, washed twice, and serial 10-fold dilutions were spotted on complete rich medium (YPD). For microscopy studies, exponentially growing cells were analyzed as described previously (Talarek et al., 2010).

Sch9 Phosphorylation Analyses

$Sch9^{T570A}$-HA_5 C-terminal phosphorylation was monitored following 2-Nitro-5-thiocyanatobenzoic acid -induced chemical cleavage as described previously (Urban et al., 2007; Wanke et al., 2008). To assess TORC1 activity upon leucine refeeding, leucine auxotrophs were starved for leucine for 90 min prior to leucine (2.8 mM) readdition for the indicated times. Quantification of TORC1 activity (extent of Sch9 phosphorylation) was determined as previously described in (Binda et al., 2009) and the TORC1 activity for Ego3-WT was set to 1.

Coimmunoprecipitation Experiments

Lysates from cells expressing untagged Gtr1-WT (Gtr1-WT) or Gtr1-WT-TAP and the other indicated EGOC fusion proteins were incubated with IgG-coated Sepharose beads (GE Healthcare). Pulled-down proteins were released by Tobacco Etch Virus (TEV) protease cleavage overnight at 4°C, precipitated with TCA/acetone, and resolved on 9% gel. Anti-TAP (Open Biosystems), anti-V5 (Invitrogen), anti-GFP (Roche), and anti-GST (Santa Cruz) antibodies along with mouse or rabbit light-chain-specific HRP-conjugated antibodies (Jackson ImmunoResearch) were used to detect Gtr1-WT-TAP, Gtr2-WT-V5, Ego3-GFP, and Ego1-GST, respectively.

ACCESSION NUMBERS

The crystal structures of the wild-type Ego3 and the Ego3-M1 mutant have been deposited with the Protein Data Bank under accession codes 4FTX and 4FUW, respectively.

SUPPLEMENTAL INFORMATION

Supplemental Information includes four tables and six figures and can be found with this article.

ACKNOWLEDGMENTS

We thank the staff members at beamline 17U of Shanghai Synchrotron Radiation Facility (SSRF), China for technical support in diffraction data collection and other members of our groups for helpful discussion. We would also like to acknowledge Vanessa Favre, Floriane Jaquier, and Sandra Huber for their technical assistance. This work was supported by grants from the National Natural Science Foundation of China (31000327 and 30900229), the Ministry of Science and Technology of China (2011CB966301 and 2011CB911102), the Chinese Academy of Sciences (2010KIP303), and the Canton of Fribourg and the Swiss National Science Foundation (to C.D.V.). T.Z. carried out the structural studies. M.-P.P.-G. carried out the functional studies. H.Y. participated in data analyses and discussion. J.D. and C.D.V. conceived the study, participated in the experimental design, data analyses, and discussion, and wrote the manuscript.

REFERENCES

Adams, P.D., Afonine, P.V., Bunkóczi, G., Chen, V.B., Davis, I.W., Echols, N., Headd, J.J., Hung, L.W., Kapral, G.J., Grosse-Kunstleve, R.W., et al. (2010). PHENIX: a comprehensive Python-based system for macromolecular structure solution. Acta Crystallogr. D Biol. Crystallogr. *66*, 213–221.

Arakawa, T., Ejima, D., Tsumoto, K., Obeyama, N., Tanaka, Y., Kita, Y., and Timasheff, S.N. (2007). Suppression of protein interactions by arginine: a proposed mechanism of the arginine effects. Biophys. Chem. *127*, 1–8.

Ashrafi, K., Farazi, T.A., and Gordon, J.I. (1998). A role for *Saccharomyces cerevisiae* fatty acid activation protein 4 in regulating protein N-myristoylation during entry into stationary phase. J. Biol. Chem. *273*, 25864–25874.

Bar-Peled, L., Schweitzer, L.D., Zoncu, R., and Sabatini, D.M. (2012). Ragulator is a GEF for the Rag GTPases that signal amino acid levels to mTORC1. Cell *150*, 1196–1208.

Binda, M., Péli-Gulli, M.P., Bonfils, G., Panchaud, N., Urban, J., Sturgill, T.W., Loewith, R., and De Virgilio, C. (2009). The Vam6 GEF controls TORC1 by activating the EGO complex. Mol. Cell *35*, 563–573.

Bonfils, G., Jaquenoud, M., Bontron, S., Ostrowicz, C., Ungermann, C., and De Virgilio, C. (2012). Leucyl-tRNA synthetase controls TORC1 via the EGO complex. Mol. Cell *46*, 105–110.

Cui, Q., Sulea, T., Schrag, J.D., Munger, C., Hung, M.N., Naïm, M., Cygler, M., and Purisima, E.O. (2008). Molecular dynamics-solvated interaction energy studies of protein-protein interactions: the MP1-p14 scaffolding complex. J. Mol. Biol. *379*, 787–802.

D'Abusco, A.S., Casadio, R., Tasco, G., Giangiacomo, L., Giartosio, A., Calamia, V., Di Marco, S., Chiaraluce, R., Consalvi, V., Scandurra, R., and Politi, L. (2005). Oligomerization of *Sulfolobus solfataricus* signature amidase is promoted by acidic pH and high temperature. Archaea *1*, 411–423.

Davis, I.W., Leaver-Fay, A., Chen, V.B., Block, J.N., Kapral, G.J., Wang, X., Murray, L.W., Arendall, W.B., 3rd, Snoeyink, J., Richardson, J.S., and Richardson, D.C. (2007). MolProbity: all-atom contacts and structure validation for proteins and nucleic acids. Nucleic Acids Res. *35*(Web Server issue), W375–W383.

De Virgilio, C., and Loewith, R. (2006). Cell growth control: little eukaryotes make big contributions. Oncogene *25*, 6392–6415.

Dubouloz, F., Deloche, O., Wanke, V., Cameroni, E., and De Virgilio, C. (2005). The TOR and EGO protein complexes orchestrate microautophagy in yeast. Mol. Cell *19*, 15–26.

Emsley, P., and Cowtan, K. (2004). Coot: model-building tools for molecular graphics. Acta Crystallogr. D Biol. Crystallogr. *60*, 2126–2132.

Gao, M., and Kaiser, C.A. (2006). A conserved GTPase-containing complex is required for intracellular sorting of the general amino-acid permease in yeast. Nat. Cell Biol. *8*, 657–667.

Gong, R., Li, L., Liu, Y., Wang, P., Yang, H., Wang, L., Cheng, J., Guan, K.L., and Xu, Y. (2011). Crystal structure of the Gtr1p-Gtr2p complex reveals new insights into the amino acid-induced TORC1 activation. Genes Dev. *25*, 1668–1673.

Guertin, D.A., and Sabatini, D.M. (2007). Defining the role of mTOR in cancer. Cancer Cell *12*, 9–22.

Han, J.M., Jeong, S.J., Park, M.C., Kim, G., Kwon, N.H., Kim, H.K., Ha, S.H., Ryu, S.H., and Kim, S. (2012). Leucyl-tRNA synthetase is an intracellular leucine sensor for the mTORC1-signaling pathway. Cell *149*, 410–424.

Hara, K., Yonezawa, K., Weng, Q.P., Kozlowski, M.T., Belham, C., and Avruch, J. (1998). Amino acid sufficiency and mTOR regulate p70 S6 kinase and eIF-4E BP1 through a common effector mechanism. J. Biol. Chem. *273*, 14484–14494.

Holm, L., and Rosenström, P. (2010). Dali server: conservation mapping in 3D. Nucleic Acids Res. *38*(Web Server issue), W545–W549.

Keith, C.T., and Schreiber, S.L. (1995). PIK-related kinases: DNA repair, recombination, and cell cycle checkpoints. Science *270*, 50–51.

Kim, D.H., Sarbassov, D.D., Ali, S.M., King, J.E., Latek, R.R., Erdjument-Bromage, H., Tempst, P., and Sabatini, D.M. (2002). mTOR interacts with raptor to form a nutrient-sensitive complex that signals to the cell growth machinery. Cell *110*, 163–175.

Kim, E., Goraksha-Hicks, P., Li, L., Neufeld, T.P., and Guan, K.L. (2008). Regulation of TORC1 by Rag GTPases in nutrient response. Nat. Cell Biol. *10*, 935–945.

Kogan, K., Spear, E.D., Kaiser, C.A., and Fass, D. (2010). Structural conservation of components in the amino acid sensing branch of the TOR pathway in yeast and mammals. J. Mol. Biol. *402*, 388–398.

Koonin, E.V., and Aravind, L. (2000). Dynein light chains of the Roadblock/LC7 group belong to an ancient protein superfamily implicated in NTPase regulation. Curr. Biol. *10*, R774–R776.

Kurzbauer, R., Teis, D., de Araujo, M.E., Maurer-Stroh, S., Eisenhaber, F., Bourenkov, G.P., Bartunik, H.D., Hekman, M., Rapp, U.R., Huber, L.A., and Clausen, T. (2004). Crystal structure of the p14/MP1 scaffolding complex: how a twin couple attaches mitogen-activated protein kinase signaling to late endosomes. Proc. Natl. Acad. Sci. USA *101*, 10984–10989.

Loewith, R., Jacinto, E., Wullschleger, S., Lorberg, A., Crespo, J.L., Bonenfant, D., Oppliger, W., Jenoe, P., and Hall, M.N. (2002). Two TOR complexes, only one of which is rapamycin sensitive, have distinct roles in cell growth control. Mol. Cell *10*, 457–468.

Lunin, V.V., Munger, C., Wagner, J., Ye, Z., Cygler, M., and Sacher, M. (2004). The structure of the MAPK scaffold, MP1, bound to its partner, p14. A complex with a critical role in endosomal map kinase signaling. J. Biol. Chem. *279*, 23422–23430.

Miertzschke, M., Koerner, C., Vetter, I.R., Keilberg, D., Hot, E., Leonardy, S., Søgaard-Andersen, L., and Wittinghofer, A. (2011). Structural analysis of the Ras-like G protein MglA and its cognate GAP MglB and implications for bacterial polarity. EMBO J. *30*, 4185–4197.

Murshudov, G.N., Vagin, A.A., and Dodson, E.J. (1997). Refinement of macromolecular structures by the maximum-likelihood method. Acta Crystallogr. D Biol. Crystallogr. *53*, 240–255.

Nada, S., Hondo, A., Kasai, A., Koike, M., Saito, K., Uchiyama, Y., and Okada, M. (2009). The novel lipid raft adaptor p18 controls endosome dynamics by anchoring the MEK-ERK pathway to late endosomes. EMBO J. *28*, 477–489.

Otwinowski, Z., and Minor, W. (1997). Processing of X-ray diffraction data collected in oscillation mode. Methods Enzymol. *276*, 307–326.

Perrakis, A., Morris, R., and Lamzin, V.S. (1999). Automated protein model building combined with iterative structure refinement. Nat. Struct. Biol. *6*, 458–463.

Reinke, A., Anderson, S., McCaffery, J.M., Yates, J., 3rd, Aronova, S., Chu, S., Fairclough, S., Iverson, C., Wedaman, K.P., and Powers, T. (2004). TOR complex 1 includes a novel component, Tco89p (YPL180w), and cooperates with Ssd1p to maintain cellular integrity in *Saccharomyces cerevisiae*. J. Biol. Chem. *279*, 14752–14762.

Reynolds, C., Damerell, D., and Jones, S. (2009). ProtorP: a protein-protein interaction analysis server. Bioinformatics *25*, 413–414.

Sancak, Y., Peterson, T.R., Shaul, Y.D., Lindquist, R.A., Thoreen, C.C., Bar-Peled, L., and Sabatini, D.M. (2008). The Rag GTPases bind raptor and mediate amino acid signaling to mTORC1. Science *320*, 1496–1501.

Sancak, Y., Bar-Peled, L., Zoncu, R., Markhard, A.L., Nada, S., and Sabatini, D.M. (2010). Ragulator-Rag complex targets mTORC1 to the lysosomal surface and is necessary for its activation by amino acids. Cell *141*, 290–303.

Schürmann, A., Brauers, A., Massmann, S., Becker, W., and Joost, H.G. (1995). Cloning of a novel family of mammalian GTP-binding proteins (RagA, RagBs, RagB1) with remote similarity to the Ras-related GTPases. J. Biol. Chem. *270*, 28982–28988.

Sekiguchi, T., Hirose, E., Nakashima, N., Ii, M., and Nishimoto, T. (2001). Novel G proteins, Rag C and Rag D, interact with GTP-binding proteins, Rag A and Rag B. J. Biol. Chem. *276*, 7246–7257.

Talarek, N., Cameroni, E., Jaquenoud, M., Luo, X., Bontron, S., Lippman, S., Devgan, G., Snyder, M., Broach, J.R., and De Virgilio, C. (2010). Initiation of the TORC1-regulated G_0 program requires Igo1/2, which license specific mRNAs to evade degradation via the 5′-3′ mRNA decay pathway. Mol. Cell *38*, 345–355.

Urban, J., Soulard, A., Huber, A., Lippman, S., Mukhopadhyay, D., Deloche, O., Wanke, V., Anrather, D., Ammerer, G., Riezman, H., et al. (2007). Sch9 is a major target of TORC1 in Saccharomyces cerevisiae. Mol. Cell *26*, 663–674.

Wanke, V., Cameroni, E., Uotila, A., Piccolis, M., Urban, J., Loewith, R., and De Virgilio, C. (2008). Caffeine extends yeast lifespan by targeting TORC1. Mol. Microbiol. *69*, 277–285.

Winn, M.D., Ballard, C.C., Cowtan, K.D., Dodson, E.J., Emsley, P., Evans, P.R., Keegan, R.M., Krissinel, E.B., Leslie, A.G., McCoy, A., et al. (2011). Overview of the CCP4 suite and current developments. Acta Crystallogr. D Biol. Crystallogr. *67*, 235–242.

Zoncu, R., Bar-Peled, L., Efeyan, A., Wang, S., Sancak, Y., and Sabatini, D.M. (2011). mTORC1 senses lysosomal amino acids through an inside-out mechanism that requires the vacuolar H(+)-ATPase. Science *334*, 678–683.

Supplemental Information

Ego3 Functions as a Homodimer to Mediate the Interaction between Gtr1-Gtr2 and Ego1 in the EGO Complex to Activate TORC1

Tianlong Zhang, Marie-Pierre Péli-Gulli, Hui Yang, Claudio De Virgilio, and Jianping Ding

Inventory of Supplemental Information

Supplementary Table S1: The table summarizes the hydrophilic and hydrophobic interactions at the dimer interface of the Ego3 homodimer, which provide supplementary information for the text of the "A unique dimer interface" section on pages 6-7.

Supplementary Table S2: The table summarizes the details of the Ego3 mutants designed in this study, which provide supplementary information for the text of the "Functional importance of the Ego3 dimer" section and the "A potential binding site for other components of the EGO complex" section on pages 12-17.

Supplementary Table S3-4: The tables summarize the plasmids and the *S. cerevisiae* strains used in this study.

Supplementary Figure S1: The figure shows the oligomeric states of the wild-type and Ego3 mutants in solution, which provide supplementary information for the text of the "Result and Discussion" section.

Supplementary Figure S2: The figure shows that sequence alignment result of Ego3 from different species and with several Roadblock/LC7 domain containing proteins, supporting Figure 1B and Figure 2.

Supplementary Figure S3: The figure indicates that the assemblies of the dimer and the tetramer are significantly different, providing supplementary information

for the text of the "Comparison of the Ego3 dimer with the Ego3 tetramer" section on pages 9-10.

Supplementary Figure S4: The figure shows the subcellular localization, sensitivity to rapamycin treatment, and TORC1 activity of the *ego3* mutants, which provide supplementary information for the text of the "Functional importance of the Ego3 dimer" section and the "A potential binding site for other components of the EGO complex" section on pages 12-17.

Supplementary Figure S5: The figure indicates that the dimer conformation of Ego3-M1 is significantly different from that of the wild-type Ego3, providing supplementary information for Figures 1A and 1C.

Supplementary Figure S6: The figure shows the conserved residues on the surface of the Ego3 dimer, which provide supplementary information for the text of the "A potential binding site for other components of the EGO complex" section on pages 16-17.

Supplementary Materials

Table S1. Hydrogen bonds and van der Waals contacts at the dimer interface of the Ego3 homodimer

(A) Hydrogen bonds

Monomer A	Location	Distance (Å)	Monomer B	Location
Lys10-N^{ζ}	α1	2.8	Tyr48-O	β2’
Thr16-$O^{\gamma 1}$	α1	2.8	Ser35-O^{γ}	β1’
Leu17-O	α1	3.4	Leu32-N	α1’/β1’ loop
Pro19-N	α1/β1 loop	3.5	Ser31-O^{γ}	α1’/β1’ loop
Tyr20-N	α1/β1 loop	2.9	Ser30-O	α1’/β1’ loop
Asp26-O	α1/β1 loop	2.8	Arg148-$N^{\eta 1}$	α3’
Asp26-O	α1/β1 loop	2.9	Arg148-$N^{\eta 2}$	α3’
Ser30-O	α1/β1 loop	3.0	Tyr20-N	α1’/β1’ loop
Ser31-O^{γ}	α1/β1 loop	3.4	Pro19-N	α1’/β1’ loop
Ser35-O^{γ}	β1	2.8	Thr16-$O^{\gamma 1}$	α1’
Tyr48-O	β2	3.0	Lys10-N^{ζ}	α1’
Asn93-O	β3	2.9	Cys95-N	β3’
Ser94-O^{γ}	β3	2.8	Tyr96-O^{η}	β3’
Cys95-N	β3	2.8	Asn93-O	β3’
Tyr96-O^{η}	β3	3.6	Tyr96-O^{η}	β3’
Tyr96-O^{η}	β3	2.8	Ser94-O^{γ}	β3’
Lys145-N^{ζ}	α3	2.9	Thr16-O	α1’
Arg148-$N^{\eta 1}$	α3	2.7	Asp26-O	α1’/β1’ loop
Arg148-$N^{\eta 2}$	α3	3.1	Asp26-O	α1’/β1’ loop
Glu152-$O^{\delta 1}$	α3	3.4	His5-$N^{\delta 1}$	N-terminal

(B) van der Waals contacts [a] (≤ 4.0 Å)

Monomer A	Location	Monomer B	Location
Val9 (4)	α1	Ile37 (1)	β1’
		Ser47 (2)	β2’
		Leu156 (1)	α3’
Lys10 (5)	α1	Ser47 (2)	β2’
		Tyr48 (3)	β2’
Phe12 (11)	α1	Ala149 (3)	α3’
		Glu152 (2)	α3’
		Leu153 (6)	α3’
Leu13 (16)	α1	Ser35 (3)	β1’
		Met36 (2)	β1’
		Ile37 (1)	β1’
		Ser47 (4)	β2’

		Tyr48 (2)	β2’
		Ala49 (3)	β2’
		Leu129 (1)	β6’
Glu14 (6)	α1	Ala49 (6)	α2’
Thr16 (10)	α1	Leu32 (4)	α1’/β1’ loop
		Ser35 (2)	β1’
		Lys145 (4)	α3’
Leu17 (14)	α1	Ser31 (3)	α1’/β1’ loop
		Leu32 (1)	L1’
		Ser34 (1)	β1’
		Ser35 (2)	β1’
		Ala49 (2)	β2’
		Thr50 (4)	β2’
		Ser51 (1)	L2’
Pro19 (6)	α1/β1 loop	Ser30 (2)	α1’/β1’ loop
		Ser31 (4)	α1’/β1’ loop
Tyr20 (14)	α1/β1 loop	Ser30 (4)	α1’/β1’ loop
		Leu141 (1)	α3’
		Lys145 (7)	α3’
		Arg148 (2)	α3’
Leu22 (7)	α1/β1 loop	Leu22 (6)	α1’/β1’ loop
		Leu141 (1)	α3’
His23 (4)	α1/β1 loop	His23 (4)	α1’/β1’ loop
Asp26 (3)	α1/β1 loop	Arg148 (3)	α3’
Phe27 (2)	α1/β1 loop	Arg148 (2)	α3’
Ser30 (7)	α1/β1 loop	Pro19 (2)	α1’/β1’ loop
		Tyr20 (5)	α1’/β1’ loop
Ser31 (7)	α1/β1 loop	Leu17 (3)	α1’
		Lys18 (1)	α1’/β1’ loop
		Pro19 (3)	α1’/β1’ loop
Leu32 (7)	α1/β1 loop	Thr16 (5)	α1’
		Leu17 (2)	α1’
Ser34 (2)	β1	Leu17 (2)	α1’
Ser35 (7)	β1	Leu13 (3)	α1’
		Thr16 (2)	α1’
		Leu17 (2)	α1’
Met36 (1)	β1	Leu13 (1)	α1’
Ile37 (2)	β1	Val9 (1)	α1’
		Leu13 (1)	α1’
Ser47 (7)	β2	Val9 (1)	α1’
		Lys10 (2)	α1’
		Leu13 (4)	α1’
Tyr48 (4)	β2	Lys10 (2)	α1’
		Leu13 (2)	α1’

Ala49 (10)	β2	Leu13 (3)	α1’
		Glu14 (4)	α1’
		Leu17 (3)	α1’
Thr50 (4)	β2	Leu17 (4)	α1’
Ser51 (1)	β2/α2 loop	Leu17 (1)	α1’
Thr87 (2)	α2/β3 loop	Glu89 (2)	α2’/β3’ loop
Glu88 (3)	α2/β3 loop	Glu89 (2)	α2’/β3’ loop
Asn93 (9)	β3	Ser94 (3)	β3’
		Cys95 (4)	β3’
		Tyr96 (2)	β3’
Ser94 (12)	β3	Asn93 (3)	β3’
		Ser94 (4)	β3’
		Tyr96 (5)	β3’
Cys95 (5)	β3	Asn93 (5)	β3’
Tyr96 (17)	β3	Asn93 (1)	β3’
		Ser94 (3)	β3’
		Tyr96 (3)	β3’
		Thr109 (2)	β4’
		Tyr139 (8)	α3’
Thr109 (2)	β4	Tyr96 (2)	β3’
Leu129 (1)	β6	Leu13 (1)	α1’
Phe131 (2)	β6	Thr16 (2)	α1’
Tyr139 (7)	α3	Tyr96 (7)	β3’
Gly140 (7)	α3	Gly140 (6)	α3’
		Ile144 (1)	α3’
Leu141 (5)	α3	Tyr20 (2)	α1’/β1’ loop
		Leu22 (1)	α1’/β1’ loop
		Ile144 (2)	α3’
Val143 (1)	α3	Tyr96 (1)	β3’
Ile144 (4)	α3	Tyr20 (1)	α1’/β1’ loop
		Gly140 (1)	α3’
		Leu141 (2)	α3’
Lys145 (10)	α3	Thr16 (3)	α1’
		Tyr20 (8)	α1’/β1’ loop
Arg148 (7)	α3	Tyr20 (1)	α1’/β1’ loop
		Val25 (2)	α1’/β1’ loop
		Asp26 (2)	α1’/β1’ loop
		Phe27 (2)	α1’/β1’ loop
Ala149 (3)	α3	Phe12 (3)	α1’
Glu152 (1)	α3	Phe12 (1)	α1’
Leu153 (5)	α3	Phe12 (5)	α1’

[a] There are a total of 264 van der Waals contacts. Number in parentheses refers to the number of van der Waals contacts the residue is involved.

Table S2. Design of the Ego3 mutants

Mutant	Mutation	Location
M0	Substitution of KPYDLHSVDFKTSSL with KPYGSTSSL	α1/β1 loop
M1	Substitution of KPYDLHSVDFKTSSL with KPYGSL	α1/β1 loop
M2	Y96E	β3
M3	M1+M2	α1/β1 loop and β3
M4	N67A/N68A/K70A/M71A	α2
M5	K77A/D78A/K79A	α2
M6	S81A/E82A/D83A/E84A	α2
M7	E111A/E113A/D114A	β4/β5 loop
M8	Deletion of the N-terminal residues 1-17	α1

Table S3. Plasmids used in this study

Plasmid	Description	Source	Figure
pRS413	*CEN, HIS3*	Ref. 1	3D; 4A-B; S4B-C
pRS414	*CEN, TRP1*	Ref. 1	3B; 3D; 4A-B; S4A-C
pRS415	*CEN, LEU2*	Ref. 1	3B; 4A; S4A-C
pRS416	*CEN, URA3*	Ref. 1	3B; 3D; 4A; S4A-B
pMPG2180	*pRS413-EGO3p-EGO3-WT-GFP*	This study	3B-C; S4A-C
YCplac33	*CEN, URA3*	Ref. 2	
pMPG2181	*pRS413-EGO3p-EGO3-M0-GFP*	This study	S4A-C
pMPG2182	*pRS413-EGO3p-EGO3-M1-GFP*	This study	3B; S4A-C
pMPG2188	*pRS413-EGO3p-EGO3-M2-GFP*	This study	S4A-C
pMPG2183	*pRS413-EGO3p-EGO3-M3-GFP*	This study	3B-C; S4A-C
pMPG2184	*pRS413-EGO3p-EGO3-M4-GFP*	This study	3B-C; S4A-C
pMPG2185	*pRS413-EGO3p-EGO3-M5-GFP*	This study	S4A-C
pMPG2189	*pRS413-EGO3p-EGO3-M6-GFP*	This study	S4A-C
pMPG2186	*pRS413-EGO3p-EGO3-M7-GFP*	This study	S4A-C
pMPG2270	*pRS413-EGO3p-EGO3-M8-GFP*	This study	3B; S4A-C
pMPG2030	*YCpLac33-EGO1p-EGO1-GST swapped to LEU2*	This study	3B-C
pJU650	*pRS416-GTR1p-GTR1-WT*	This study	3C
pMB1344	*YCpLac33-GTR1p-GTR1-WT-TAP*	Ref. 3	3B-C
pMPG2177	*pRS414-GTR2p-GTR2-WT-V5-6HIS*	This study	3B-C
pJU1030	*pRS416-SCH9p-SCH9*^{T570A}*-HA*$_5$	Ref. 4	4A-B; S4C
pMPG2280	*pRS413-EGO3p-EGO3-WT*	This study	3D; 4A-B
pMPG2298	*pRS413-EGO3p-EGO3-M1*	This study	3D; 4A-B
pMPG2279	*pRS413-EGO3p-EGO3-M3*	This study	3D; 4A-B
pMPG2261	*pRS413-EGO3p-EGO3-M4*	This study	3D; 4A-B
pMPG2271	*pRS413-EGO3p-EGO3-M8*	This study	3D; 4A-B
p1559	*pDL2-Alg5*	Dualsystems	3A
p1571	*pCabWT*	Dualsystems	3A
pMPG2220	*pCabWT-EGO3-WT*	This study	3A
pMPG2265	*pCabWT-EGO3-M1*	This study	3A
pMPG2267	*pCabWT-EGO3-M3*	This study	3A
pMPG2268	*pCabWT-EGO3-M4*	This study	3A
pMPG2269	*pCabWT-EGO3-M8*	This study	3A

p1558	*pPR3-N*	Dualsystems	
pMPG2221	*pPR3-N-EGO3-WT*	This study	3A
pMPG2255	*pPR3-N-EGO3-M1*	This study	3A
pMPG2257	*pPR3-N-EGO3-M3*	This study	3A
pMPG2258	*pPR3-N-EGO3-M4*	This study	3A
pMPG2259	*pPR3-N-EGO3-M8*	This study	3A
pNP1696	*pPR3-N-EGO1*	Ref. 3	3A
pNP1691	*pPR3-N-GTR1-Q65L (GTP)*	Ref. 3	3A
pNP1694	*pPR3-N-GTR2-Q66L (GTP)*	This study	3A

Table S4. *S. cerevisiae* strains used in this study

Strain	Genotype	Source	Figure
KT1960	*MATα his3 leu2 ura3 trp1*	Ref. 4	
KT1961	*MATa his3 leu2 ura3 trp1*	Ref. 4	4A-B; S1B-C
MPG2650	*MATa ego3Δ::KanMX his3 leu2 ura3 trp1*	This study	3B; 4A-B; S1A-C
MPG2761	*MATa ego1Δ::KanMX ego3Δ::KanMX gtr1Δ::natMX gtr2Δ::natMX his3 leu2 ura3 trp1*	This study	3B-C
MPG2963	*MATa LEU2::GTR1-WT-GFP ego3Δ::KanMX gtr1Δ::natMX4 his3 ura3-52 leu2 trp1*	This study	3D
NMY51	*MATa his3Δ200 trp1-901 leu2-3,112 ade2 LYS::(lexAop)4-HIS3 ura3::(lexAop)8- lacZ ade2::(lexAop)8-ADE2 GAL4*	Dualsystems	
MPG2952	*MATa ego3Δ::KanMX his3Δ200 trp1-901 leu2-3,112 ade2 LYS::(lexAop)4-HIS3 ura3::(lexAop)8- lacZ ade2::(lexAop)8-ADE2 GAL4*	This study	3A

Supplementary Figure legends

Figure S1. Analyses of the oligomeric states of the wild-type and Ego3 mutants in solution by size-exclusion chromatography. Absorbance at 280 nm is plotted against the elution volume. Positions of the molecular mass standards are indicated. The curves for Ego3-WT, Ego3-M0, Ego3-M1, and Ego3-M4 are colored in red, blue, pink, and green, respectively.

Figure S2. Sequence comparison of Ego3 from different species and with several Roadblock/LC7 domain containing proteins. (A) Sequence alignment of Ego3 from different species. The sequences include *Saccharomyces cerevisiae*, *Lachancea thermotolerans*, *Vanderwaltozyma polyspora*, *Zygosaccharomyces rouxii*, *Ashbya gossypii*, and *Candida glabrata*. The secondary structures of *S. cerevisiae* Ego3 are placed above the alignment. Tyr96 and Arg148 that are involved in the dimer interface are indicated with a star and a triangle, respectively. The sequence alignments were performed using the program ESPript (Ref. 5). The secondary structures of *S. cerevisiae* Ego3 were also determined by ESPript. (B) Structure-based sequence alignment of Ego3 with several Roadblock/LC7 domain containing proteins. The secondary structures of Ego3 are placed above the alignment and those of p14 are placed below the alignment. The residues in the α1/β1 loop are underlined. The sequence alignments were performed using the program ESPript.

Figure S3. Structural comparison of the dimeric interface in the Ego3 dimer and the Ego3 tetramer. (A) Ribbon representation of the Ego3 tetramer, which is colored with monomers A and C in green and monomers B and D in blue, respectively. The zoom-in window shows the interactions between the two β3 strands of monomers A and B. Hydrogen bonds are indicated with dashed lines. (B) Superposition of the Ego3 homodimer and the A/B dimer in the Ego3 homotetramer. The Ego3 homodimer is colored with one monomer in yellow and the other in cyan; monomers A and B in the Ego3 homotetramer are colored in green and blue, respectively. When one monomer is superimposed, the other monomer would have a rotation of 116° relative to each other.

Figure S4. Initial characterization of the *ego3* mutants. (A) Subcellular localization of the Ego3-GFP variants. (B) Response of the *ego3* mutants to rapamycin treatment. Serial 10-fold dilutions were spotted on complete rich medium (YPD) supplemented with vehicle (veh.) or the indicated concentrations of rapamycin. Alternatively, they were treated for 6 hrs with 200 ng/ml rapamycin, washed twice, spotted on YPD (Rap recovery), and grown for 2 days at 30°C. (C) TORC1 activity in exponentially growing *ego3* mutants. *In vivo* TORC1 activity was assessed by monitoring the phosphorylation level of the TORC1 substrate Sch9 in the indicated prototrophic strains. Numbers below represent TORC1 activity in exponentially growing cells. TORC1 activity in *ego3*Δ cells expressing Ego3-WT-GFP served as a reference and was set to 1.

Figure S5. Structural comparison of Ego3-WT and Ego3-M1. The color coding of the monomers is the same as in Figure 1. When one monomer is superimposed, the other in the Ego3-M1 dimer rotates ~86° relative to that in the Ego3-WT dimer.

Figure S6. Distribution of the conserved residues on the surface of the Ego3 dimer. The strictly conserved, conserved, and less conserved residues are colored in orange, pink, and gray, respectively.

References

1 Brachmann CB *et al.* (1998). Designer deletion strains derived from *Saccharomyces cerevisiae* S288C: a useful set of strains and plasmids for PCR-mediated gene disruption and other applications. *Yeast* **14**: 115-132.

2 Gietz RD, Sugino A (1988). New yeast-*Escherichia coli* shuttle vectors constructed with *in vitro* mutagenized yeast genes lacking six-base pair restriction sites. *Gene* **74**: 527-534.

3 Binda M *et al.* (2009). The Vam6 GEF controls TORC1 by activating the EGO complex. *Mol. Cell* **35**: 563-573.

4 Urban J *et al.* (2007). Sch9 is a major target of TORC1 in *Saccharomyces cerevisiae*. *Mol. Cell* **26**: 663-674.

5 Pedruzzi I *et al.* (2003). TOR and PKA signaling pathways converge on the protein kinase Rim15 to control entry into G_0. *Mol. Cell* **12**: 1607-1613.

6 Gouet P, Courcelle E, Stuart DI, Metoz F (1999). ESPript: analysis of multiple sequence alignments in PostScript. *Bioinformatics* **15**: 305-308.

Figure S1

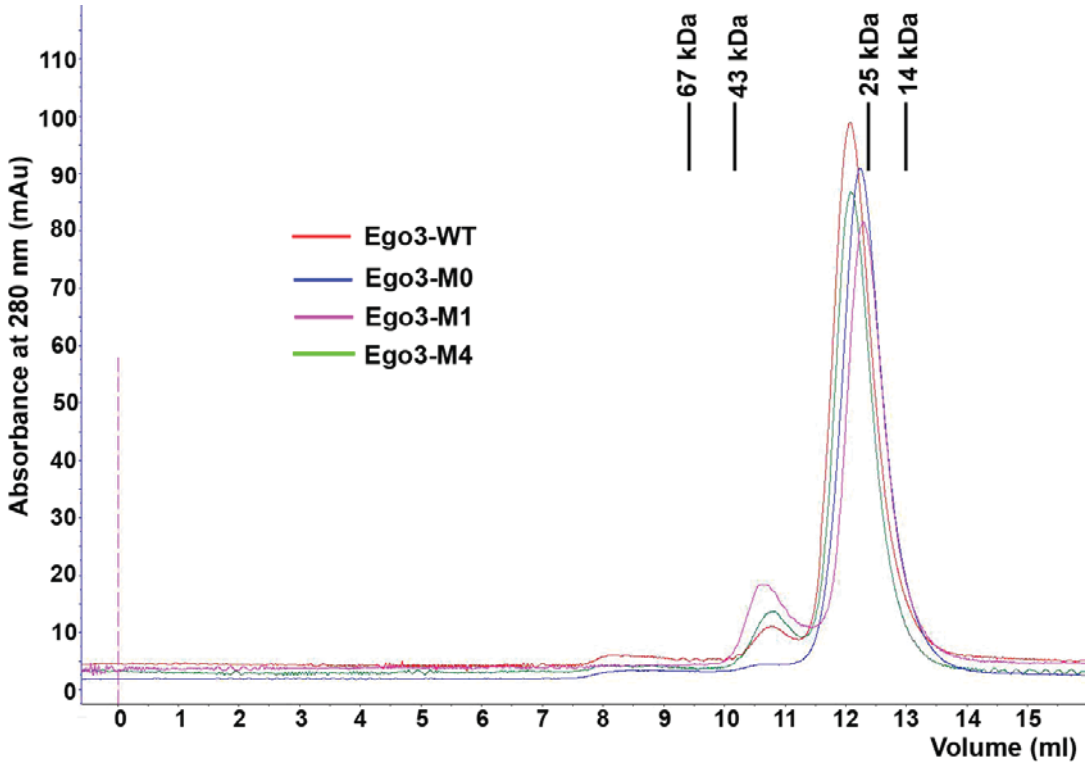

Figure S2

A

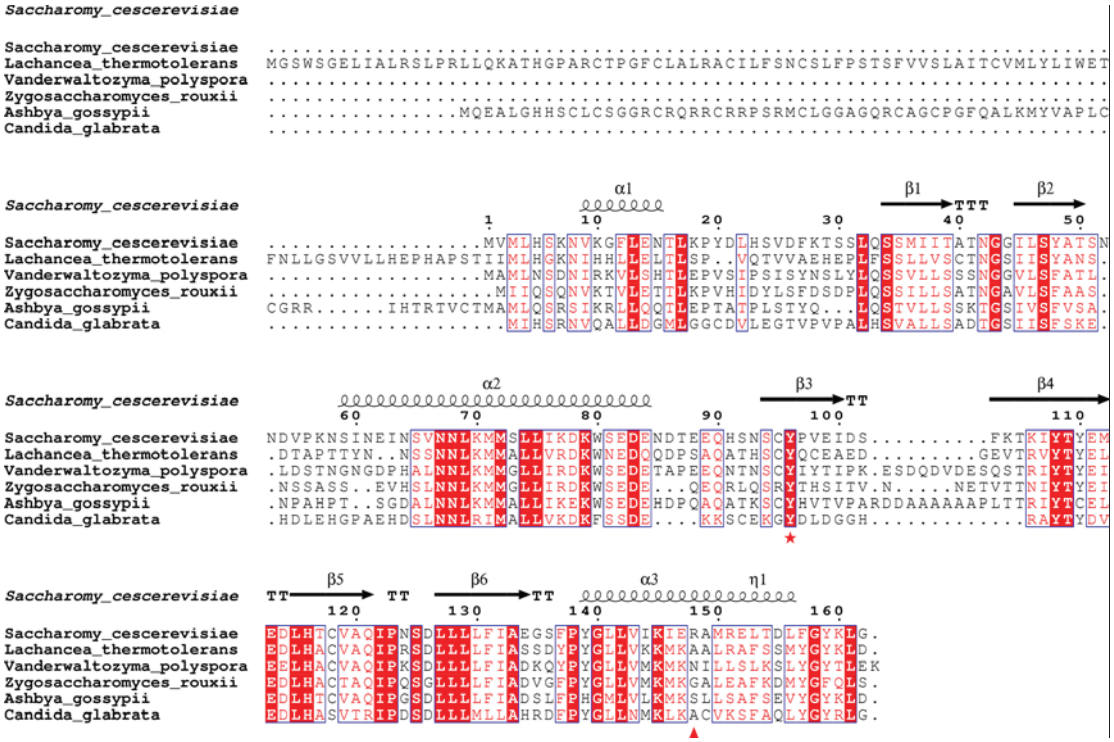

B

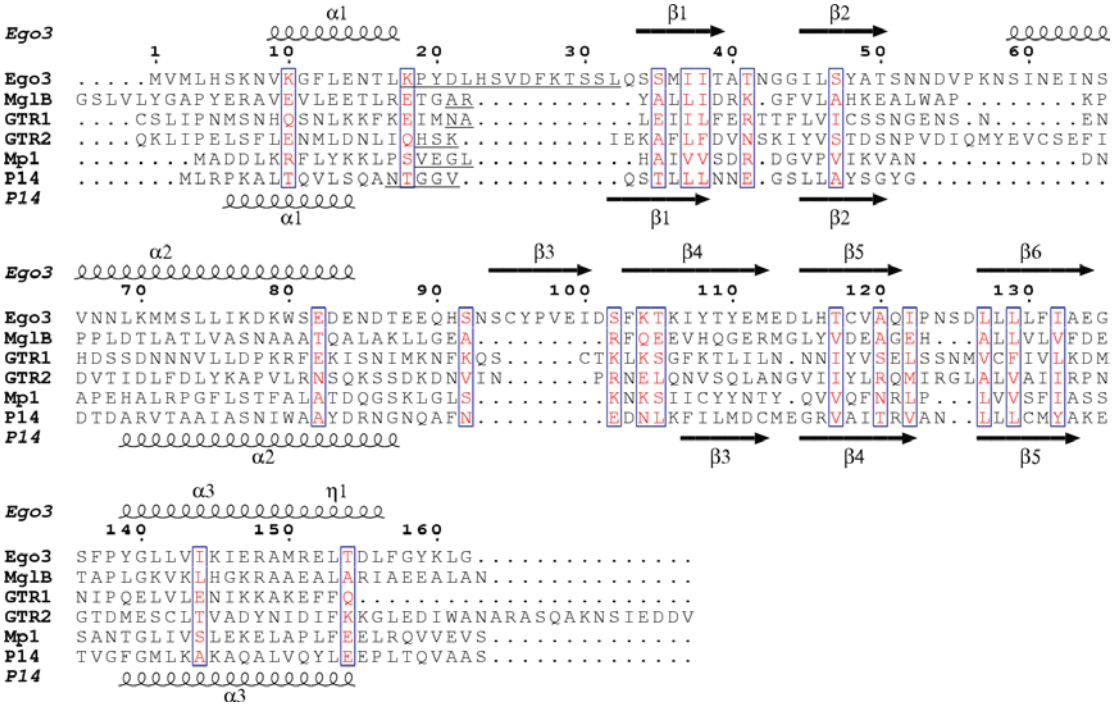

Figure S3

A

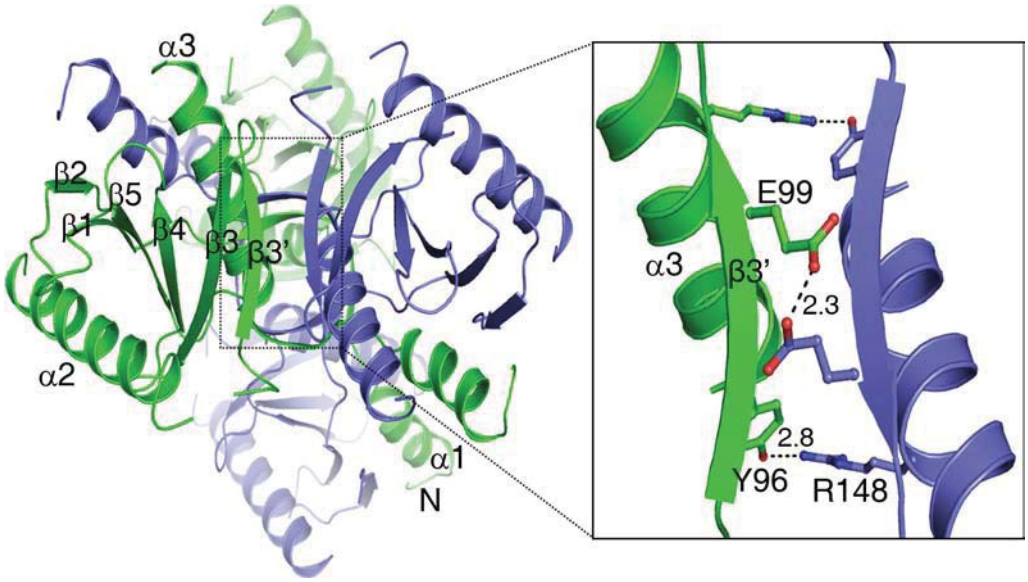

B

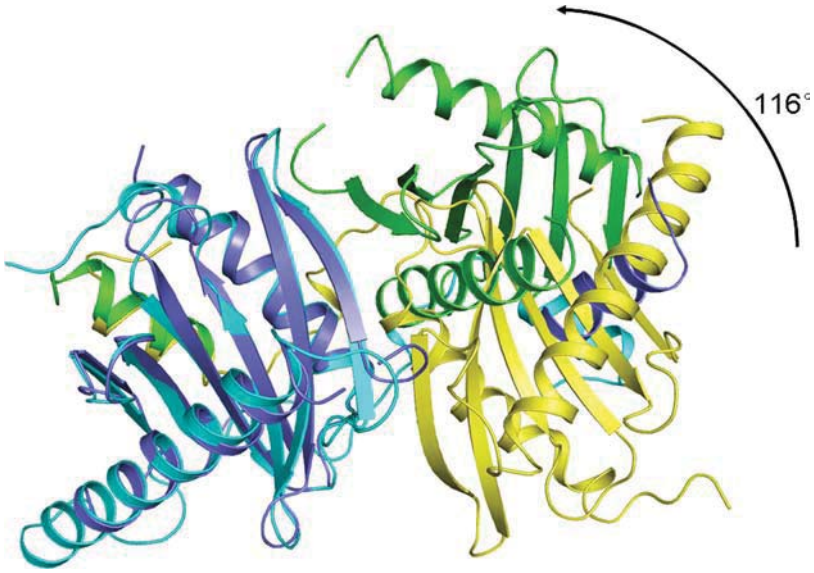

Figure S4

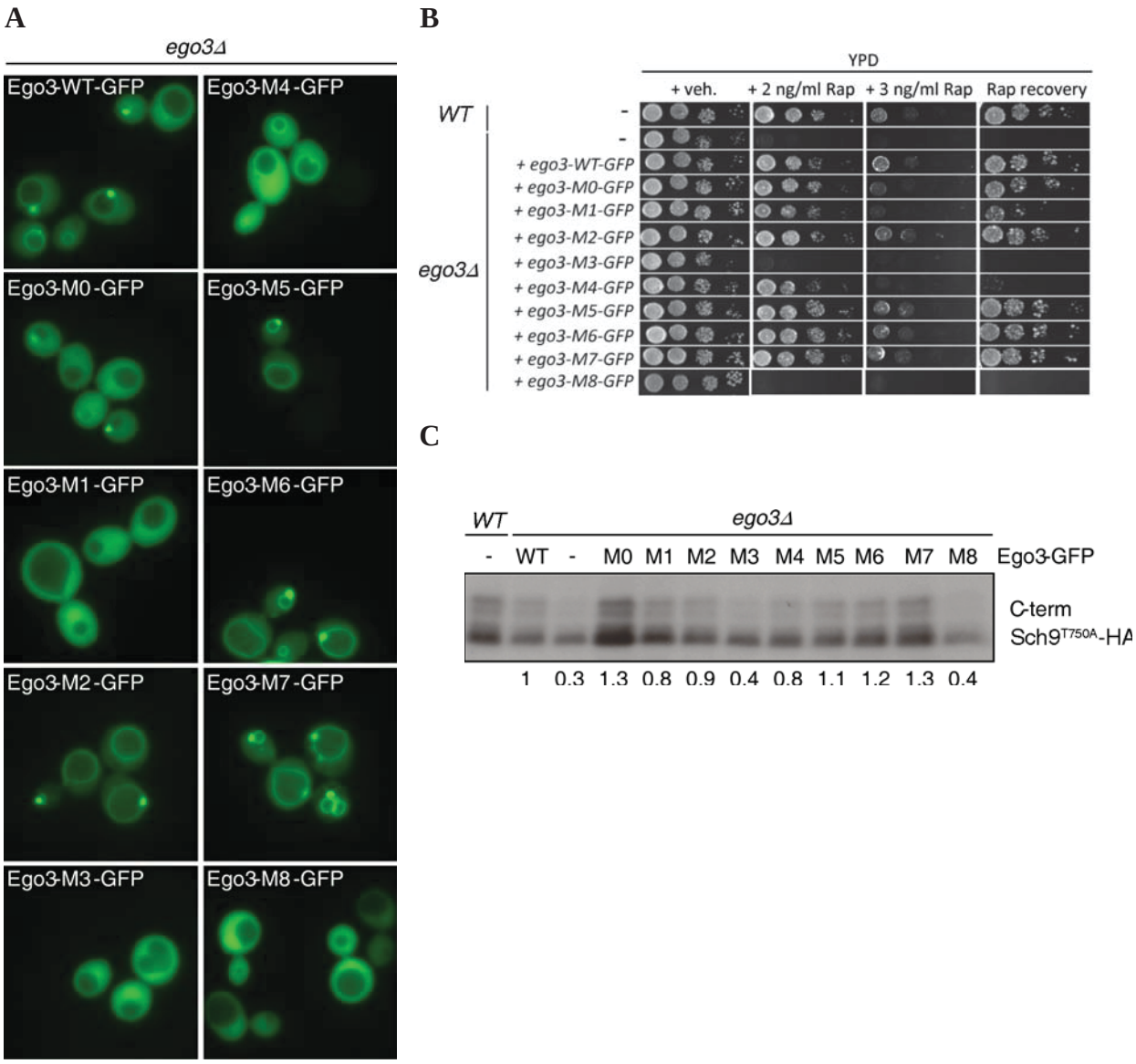

Figure S5

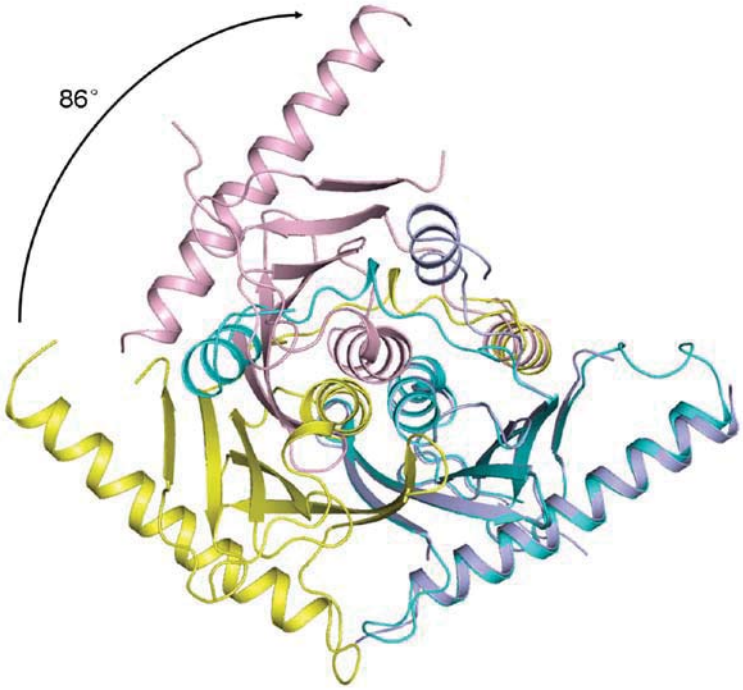

Figure S6